Supplemental Information: Pattern formation of lipid domains in bilayer membranes

Qiwei Yu[1] and Andrej Košmrlj[2,3]

[1] *Lewis-Sigler Institute for Integrative Genomics, Princeton University, Princeton, NJ 08544*
[2] *Department of Mechanical and Aerospace Engineering, Princeton University, Princeton, NJ 08544*
[3] *Princeton Materials Institute, Princeton University, Princeton, NJ 08544*

CONTENTS

I. ANALYTICAL SOLUTION OF THE MODEL

A. Dynamical equations for deformation and composition

We start with the full free energy

$$\mathcal{F}[h,\phi_1,\phi_2] = \mathcal{F}_e[h,\phi_1] + \mathcal{F}_c[\phi_1,\phi_2] = \int \left[\frac{1}{2}\sigma(\nabla h)^2 + \frac{1}{2}\kappa\big(\nabla^2 h - c_1\phi_1\big)^2\right] \mathrm{d}^2\boldsymbol{r} + \int \left[\sum_{i=1}^{3}\phi_i \ln\phi_i + \sum_{i\neq j}\chi_{i,j}\big(\phi_i\phi_j - \lambda^2\nabla\phi_i\cdot\nabla\phi_j\big) + \xi\phi_1\phi_2\phi_3\right] \mathrm{d}^2\boldsymbol{r}\,. \tag{S1}$$

Membrane height field $h(\boldsymbol{r})$ follows the Model A dynamics (not conserved) and volume fractions of molecules $\phi_{1,2}(\boldsymbol{r})$ follow the Model B dynamics (conserved)

$$\frac{\partial h}{\partial t} = -M_h\frac{\delta F}{\delta h}, \tag{S2}$$

$$\frac{\partial \phi_i}{\partial t} = M_i\nabla^2\frac{\delta F}{\delta \phi_i}. \tag{S3}$$

The volume fraction of the last component $\phi_3 = 1-\phi_1-\phi_2$ is dependent on $\phi_{1,2}$ by incompressibility. As mentioned in the main text, we nondimensionalize all the parameters: space and time are measured in units of λ and nk_BTM/λ^2, respectively, and energy is measured in units of nk_BT. Hence, we set $M=1$ and $\lambda=1$ in the following derivation. The equations of motion are

$$\frac{\partial h}{\partial t} = \sigma\nabla^2 h - \kappa\nabla^4 h + \kappa c_1\nabla^2\phi_1, \tag{S4}$$

$$\frac{\partial \phi_1}{\partial t} = \kappa c_1^2\nabla^2\phi_1 - \kappa c_1\nabla^4 h + \nabla^2\frac{\delta \mathcal{F}_c}{\delta \phi_1}, \tag{S5}$$

$$\frac{\partial \phi_2}{\partial t} = \nabla^2\frac{\delta \mathcal{F}_c}{\delta \phi_2}. \tag{S6}$$

where $\frac{\delta \mathcal{F}_c}{\delta \phi_{1,2}}$ are the chemical potentials due to the (generalized) Flory-Huggins free energy:

$$\frac{\delta \mathcal{F}_c}{\delta \phi_1} = \ln\left(\frac{\phi_1}{1-\phi_1-\phi_2}\right) + (\chi_{12}-\chi_{23})(1+\nabla^2)\phi_2 + \chi_{13}(1+\nabla^2)(1-2\phi_1-\phi_2) + \xi\phi_2(1-2\phi_1-\phi_2), \tag{S7}$$

$$\frac{\delta \mathcal{F}_c}{\delta \phi_2} = \ln\left(\frac{\phi_2}{1-\phi_1-\phi_2}\right) + (\chi_{12}-\chi_{13})(1+\nabla^2)\phi_1 + \chi_{23}(1+\nabla^2)(1-\phi_1-2\phi_2) + \xi\phi_1(1-\phi_1-2\phi_2). \tag{S8}$$

B. Pattern size and morphology

Fourier transforming Eq. (S4) yields the steady-state solution for h:

$$h(\boldsymbol{k}) = -\frac{\kappa c_1}{\kappa k^2+\sigma}\phi_1(\boldsymbol{k}). \tag{S9}$$

Let $\delta\phi_i = \phi_i - \bar{\phi}_i$. The free energy for membrane deformation reduces to

$$\mathcal{F}_e[h,\phi_1] = \int \left[\frac{1}{2}\sigma(\nabla h)^2 + \frac{1}{2}\kappa\big(\nabla^2 h - c_1\bar{\phi}_1 - c_1\delta\phi_1\big)^2\right] \mathrm{d}^2\boldsymbol{r} \tag{S10}$$

$$= \frac{A}{2}\kappa c_1^2 \bar{\phi_1}^2 + \int \frac{\mathrm{d}^2\boldsymbol{k}}{(2\pi)^2}\left[\frac{1}{2}(\sigma+\kappa k^2)k^2 h(\boldsymbol{k})h(-\boldsymbol{k}) + \frac{1}{2}\kappa c_1^2\delta\phi_1(\boldsymbol{k})\delta\phi_1(-\boldsymbol{k}) + \kappa c_1 k^2\bar{\phi}_1\delta\phi_1(-\boldsymbol{k})h(\boldsymbol{k})\right] \tag{S11}$$

$$= \frac{A}{2}\kappa c_1^2 \bar{\phi_1}^2 + \frac{1}{2}\kappa c_1^2 \int \frac{|\delta\phi_1(\boldsymbol{k})|^2}{1+\frac{\kappa k^2}{\sigma}}\frac{\mathrm{d}^2\boldsymbol{k}}{(2\pi)^2}, \tag{S12}$$

where A is the total area of the membrane.

Assuming phase separation along the tie lines of $\mathcal{F}_c$ (which can be determined by the convex hull construction [1]), the ratio of the concentration change of the two phospholipid species: $s = -\delta\phi_2/\delta\phi_1$.

$$\mathcal{F}_c[\phi_1,\phi_2] = A f_c(\bar{\phi}_1,\bar{\phi}_2) + \int \left[-\frac{a}{2}\delta\phi_1^2 + \frac{c}{3}\delta\phi_1^3 + \frac{b}{4}\delta\phi_1^4 + \frac{1}{2}\mu(\nabla\delta\phi_1)^2\right]\mathrm{d}^2\boldsymbol{r}\,, \tag{S13}$$

The expansion parameters are:

$$\mu = 2(s\chi_{12} - (s-1)\chi_{13} + s(s-1)\chi_{23}), \tag{S14}$$

$$a = -\left(\bar{\phi}_1^{-1} + s^2\bar{\phi}_2^{-1} + (s-1)^2\bar{\phi}_3^{-1}\right) + \mu + 2\xi\big[s(s-1)\bar{\phi}_1 - (s-1)\bar{\phi}_2 + s\bar{\phi}_3\big], \tag{S15}$$

$$c = \frac{1}{2}\big(-\bar{\phi}_1^{-2} + s^3\bar{\phi}_2^{-2} - (s-1)^3\bar{\phi}_3^{-2} - 6s(s-1)\xi\big), \tag{S16}$$

$$b = \frac{1}{3}\big(\bar{\phi}_1^{-3} + s^4\bar{\phi}_2^{-3} + (s-1)^4\bar{\phi}_3^{-3}\big). \tag{S17}$$

Here, μ is related to the line tension between the two phases. In the absence of membrane deformation ($h = 0$), phase separation requires $a > 0$. Note that $b > 0$ ensures that $\delta\phi_1$ remains bounded.

Combining Eq. (S12) and Eq. (S13) leads to the total free energy given by Eq. (7) of the main text (shifting the zero of the free energy by σA to include the surface energy of the undeformed membrane):

$$\begin{aligned}\mathcal{F}_{\mathrm{eff}}[\delta\phi_1] = \left[\sigma + f_c(\bar{\phi}_1,\bar{\phi}_2) + \frac{1}{2}\kappa c_1^2\bar{\phi}_1^2\right]A + \frac{1}{2}\int\left(\frac{\sigma\kappa c_1^2}{\sigma+\kappa k^2} + \mu k^2\right)|\delta\phi_1(\boldsymbol{k})|^2\frac{\mathrm{d}^2\boldsymbol{k}}{(2\pi)^2} \\ + \int\left[-\frac{a}{2}\delta\phi_1(\boldsymbol{r})^2 + \frac{c}{3}\delta\phi_1(\boldsymbol{r})^3 + \frac{b}{4}\delta\phi_1(\boldsymbol{r})^4\right]\mathrm{d}^2\boldsymbol{r}\,.\end{aligned} \tag{S18}$$

The first term gives the effective surface energy $\sigma_{\mathrm{eff}} = \sigma + f_c(\bar{\phi}_1,\bar{\phi}_2) + \frac{1}{2}\kappa c_1^2\bar{\phi}_1^2$ [Eq. (8) of the main text]. Minimizing the free energy with respect to $|\boldsymbol{k}|$ leads to $k^2 = k_c^2 = \sqrt{\frac{\sigma c_1^2}{\mu}} - \frac{\sigma}{\kappa}$ [Eq. (9) of the main text]. Expanding the free energy around k_c:

$$\frac{\sigma\kappa c_1^2}{\sigma+\kappa k^2} + \mu k^2 = 2\sqrt{\mu\sigma c_1^2} - \frac{\sigma\mu}{\kappa} + \sqrt{\frac{\mu^3}{\sigma c_1^2}}\big(k^2-k_c^2\big)^2 + O\big[(k^2-k_c^2)^3\big]. \tag{S19}$$

Thus, the dynamical equation for ϕ_1 is

$$\frac{\partial \delta\phi_1}{\partial t} = \nabla^2 \frac{\delta \mathcal{F}}{\delta \phi_1} = \nabla^2 \left[\left(-a_{\text{eff}} + \sqrt{\frac{\mu^3}{\sigma c_1^2}} \left(k_c^2 + \nabla^2\right)^2 \right) \delta\phi_1 + c\delta\phi_1^2 + b\delta\phi_1^3 \right], \tag{S20}$$

where

$$a_{\text{eff}} = a - 2\sqrt{\mu\sigma c_1^2} + \frac{\sigma\mu}{\kappa}. \tag{S21}$$

Eq. (S20) has the same form as the conserved (or derivative) Swift-Hohenberg equation [2–4]. Applying amplitude expansion $\delta\phi_1 = \phi_1 - \bar{\phi_1} = \sum_n A_n e^{i\boldsymbol{k}_n \cdot \boldsymbol{r}} + \text{c.c.}$ with $|k_n| = k_c$ and $n = 3$ (i.e., the wavevectors $\boldsymbol{k}_{1,2,3}$ are of the same magnitude and oriented at 120 degrees with respect to each other) leads to the amplitude equations:

$$\frac{\mathrm{d}A_1}{\mathrm{d}\tau} = \left(a_{\text{eff}} - 3b|A_1|^2 - 6b|A_2|^2 - 6b|A_3|^2\right) A_1 - 2cA_2^* A_3^*, \tag{S22}$$

$$\frac{\mathrm{d}A_2}{\mathrm{d}\tau} = \left(a_{\text{eff}} - 3b|A_2|^2 - 6b|A_1|^2 - 6b|A_3|^2\right) A_2 - 2cA_1^* A_3^*, \tag{S23}$$

$$\frac{\mathrm{d}A_3}{\mathrm{d}\tau} = \left(a_{\text{eff}} - 3b|A_3|^2 - 6b|A_1|^2 - 6b|A_2|^2\right) A_3 - 2cA_1^* A_2^*. \tag{S24}$$

where $\tau = k_c^2 t$. Let $A_i = R_i \exp(i\theta_i)$. The dynamics of the amplitude R and phase θ are given by

$$\frac{\dot{R}_1}{R_1} = \frac{\mathrm{d}\ln R_1}{\mathrm{d}\tau} = \mathrm{Re}\left\{ \frac{\mathrm{d}\ln A_1}{\mathrm{d}\tau} \right\} = a_{\text{eff}} - 3bR_1^2 - 6bR_2^2 - 6bR_3^2 - 2c\frac{R_2 R_3}{R_1}\cos(\theta_1 + \theta_2 + \theta_3), \tag{S25}$$

$$\dot{\theta_1} = \frac{\mathrm{d}\theta_1}{\mathrm{d}\tau} = \mathrm{Im}\left\{ \frac{\mathrm{d}\ln A_1}{\mathrm{d}\tau} \right\} = 2c\frac{R_2 R_3}{R_1}\sin(\theta_1 + \theta_2 + \theta_3). \tag{S26}$$

The sum of phases $\Theta = \theta_1 + \theta_2 + \theta_3$ evolves following

$$\frac{\mathrm{d}\Theta}{\mathrm{d}\tau} = 2cQ\sin\Theta, \quad \text{where } Q = \sum_{\text{cyc.}} \frac{R_{i+1}R_{i+2}}{R_i} > 0, \tag{S27}$$

where cyc. represents cyclic summation over indices $i = 1, 2, 3$. Thus, Θ has two fixed points $\Theta = 0$ and $\Theta = \pi$. However, only the one corresponding to $\cos\Theta = -\text{sgn}(c)$ is stable. Substituting it to the amplitude equation for R_1 leads to

$$\frac{\mathrm{d}R_1}{\mathrm{d}\tau} = R_1 \left(a_{\text{eff}} - 3bR_1^2 - 6bR_2^2 - 6bR_3^2 + 2|c|\frac{R_2 R_3}{R_1} \right). \tag{S28}$$

The fixed points of this equation represents different patterns. To analyze the stability of the fixed points, we also compute the Jacobian:

$$J = \frac{\partial \dot{R}}{\partial R} = \begin{pmatrix} a_{\text{eff}} - 9bR_1^2 - 6bR_2^2 - 6bR_3^2 & -12bR_1R_2 + 2|c|R_3 & -12bR_1R_3 + 2|c|R_2 \\ -12bR_1R_2 + 2|c|R_3 & a_{\text{eff}} - 9bR_2^2 - 6bR_1^2 - 6bR_3^2 & -12bR_2R_3 + 2|c|R_1 \\ -12bR_1R_3 + 2|c|R_2 & -12bR_2R_3 + 2|c|R_1 & a_{\text{eff}} - 9bR_3^2 - 6bR_1^2 - 6bR_2^2 \end{pmatrix}. \tag{S29}$$

This equation has three fixed points:

- Uniform state: $R_1 = R_2 = R_3 = 0$. The fixed point is stable when $a_{\text{eff}} < 0$.
- Stripe state: $R_1 = \sqrt{\frac{a_{\text{eff}}}{3b}}$ and $R_2 = R_3 = 0$. The Jacobian is

$$J = \begin{pmatrix} -2a_{\text{eff}} & 0 & 0 \\ 0 & -a_{\text{eff}} & 2|c|\sqrt{\frac{a_{\text{eff}}}{3b}} \\ 0 & 2|c|\sqrt{\frac{a_{\text{eff}}}{3b}} & -a_{\text{eff}} \end{pmatrix}. \tag{S30}$$

The fixed point is stable when the eigenvalues have negative real parts, which requires

$$a_{\text{eff}}^2 - 4c^2\frac{a_{\text{eff}}}{3b} > 0 \Rightarrow \frac{a_{\text{eff}}b}{c^2} > \frac{4}{3}. \tag{S31}$$

- Dots (hexagonal) state: $R_1 = R_2 = R_3 = R$, which is given by

$$a_{\text{eff}} + 2|c|R - 15bR^2 = 0 \Rightarrow R_\pm = \frac{|c| \pm \sqrt{c^2 + 15a_{\text{eff}}b}}{15b} = \frac{|c|}{15b}\left(1 \pm \sqrt{1 + \frac{15a_{\text{eff}}b}{c^2}}\right). \tag{S32}$$

  The solution exists when $a_{\text{eff}} > -\frac{c^2}{15b}$. By computing the eigenvalues of the Jacobian, it can be shown that R_- is always an unstable fixed point, while R_+ is stable when $a_{\text{eff}} < \frac{16c^2}{3b}$.

Combining the above results, we find that the stability of the fixed points can be captured by a single control parameter $g = \frac{a_{\text{eff}}b}{c^2} \equiv \frac{b}{c^2}\left(a - 2\sqrt{c_1^2\sigma\mu} + \frac{\mu\sigma}{\kappa}\right)$. The uniform state is stable when $g < 0$, the stripe state is stable when $g > \frac{4}{3}$, and the dots state is stable when $-\frac{1}{15} < g < \frac{16}{3}$.

C. Total free energy density

Here, we present the free energy density of the patterns, which is used in Fig. 3 of the main text. Following Eq. (S18), the free energy density of the system is given by

$$f = f_0 - \frac{a_{\text{eff}}}{2}\left\langle \delta\phi_1^2 \right\rangle + \frac{c}{3}\left\langle \delta\phi_1^3 \right\rangle + \frac{b}{4}\left\langle \delta\phi_1^4 \right\rangle, \tag{S33}$$

where f_0 is the free energy density of the uniform state, and $\langle\cdot\rangle$ represents spatial averaging over the entire system.

For the stripe state, we have:

$$\left\langle \phi^2 \right\rangle = 2R^2 = \frac{2a_{\text{eff}}}{3b}, \quad \left\langle \phi^3 \right\rangle = 0, \quad \left\langle \phi^4 \right\rangle = 6R^4 = \frac{2a_{\text{eff}}^2}{3b^2}. \tag{S34}$$

$$f_{\text{stripe}} = f_0 - \frac{a_{\text{eff}}}{2}\frac{2a_{\text{eff}}}{3b} + \frac{b}{4}\frac{2a_{\text{eff}}^2}{3b^2} = f_0 - \frac{a_{\text{eff}}^2}{6b}. \tag{S35}$$

For the dot state, we have:

$$\left\langle \phi^2 \right\rangle = 6R^2, \quad \left\langle \phi^3 \right\rangle = -12R^3\text{sgn}(c), \quad \left\langle \phi^4 \right\rangle = 90R^4. \tag{S36}$$

$$f_{\text{dot}} = f_0 - R^2\left(|c|R + \frac{3}{2}a_{\text{eff}}\right), \quad \text{where} \quad R = \frac{|c|}{15b}\left(1 + \sqrt{1 + \frac{15a_{\text{eff}}b}{c^2}}\right). \tag{S37}$$

D. Validity of the tie line approximation

In order to justify expanding the free energy along the tie line, we plot the histogram of local composition $(\phi_1(r), \phi_2(r))$ and compare it with the tie line. Fig. S1 shows the histograms for the 4 steady-state patterns shown in Fig. 1C of the main text. Indeed, the histograms are peaked around the tie line, which justifies fixing the ratio $s = -\delta\phi_2/\delta\phi_1$ to that of the tie line.

E. Using analytical μ to predict characteristic domain size

In Fig. 2C,D of the main text, the characteristic domain size was captured with a single fitting parameter μ. This parameter can also be estimated from Eq. (S14), which leads to slightly worse agreement (see Fig. S2).

II. DETAILS OF THE NUMERICAL SIMULATIONS

The dynamical equations Eq. (S4)–(S6) are solved in a $L \times L$ square domain with periodic boundary conditions. Space is discretized into $N \times N$ grid points, and time is discretized to steps of Δt. Time integration is performed in the Fourier space $y_i^n(\boldsymbol{k}) = \int y_i^n(\boldsymbol{r})\exp(-i\boldsymbol{k}\cdot\boldsymbol{r})\mathrm{d}^2\boldsymbol{r}$ using an implicit-explicit scheme:

$$\frac{\boldsymbol{y}^{n+1}(\boldsymbol{k}) - \boldsymbol{y}^n(\boldsymbol{k})}{\Delta t} = \boldsymbol{L}[\boldsymbol{y}^{n+1}(\boldsymbol{k})] + \boldsymbol{N}[\boldsymbol{y}^n(\boldsymbol{k})], \tag{S38}$$

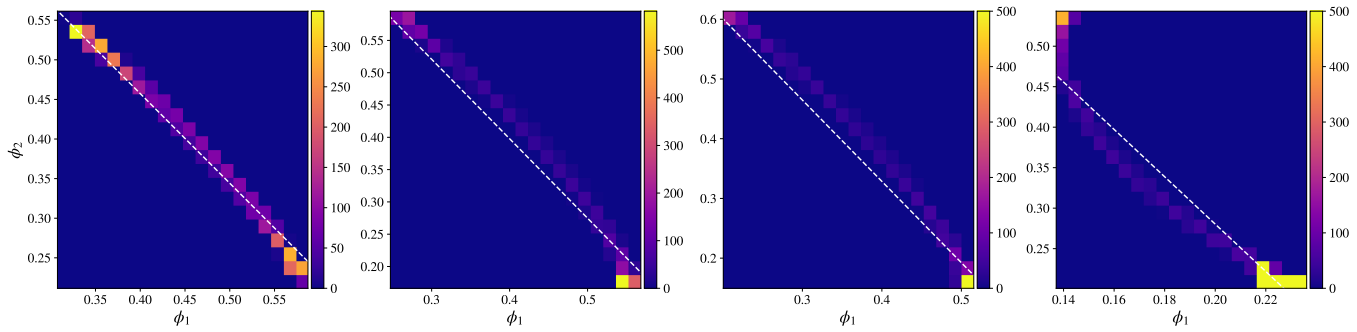

FIG. S1. The probability density function (PDF) of the local composition $P(\phi_1, \phi_2)$ for the 4 steady-state patterns shown in Fig. 1C of the main text (from left to right are the PDFs corresponding to the upper left, upper right, lower left, and lower right panels of Fig. 1C). The white dashed lines are the tie lines obtained from the convex hull construction. For the last two panels, the color bar is truncated at 500 to make the distribution visible.

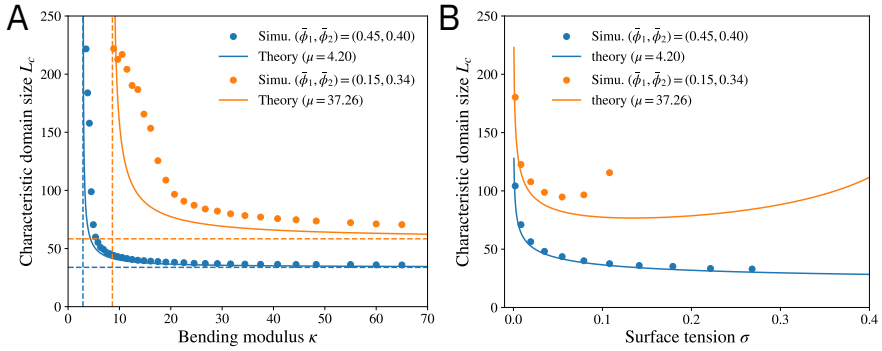

FIG. S2. The characteristic domain size as functions of (A) the bending modulus κ and (B) surface tension σ. The parameters are the same as Fig. 2C,D of the main text, except for μ which is estimated from Eq. (S14) rather than obtained by fitting.

where $\boldsymbol{y} = (h, \phi_1, \phi_2)^T$ and n labels the time steps. $\boldsymbol{L}(\boldsymbol{y}) = \mathbf{A} \cdot \boldsymbol{y}$ is the linear and implicit part of the equation and $\boldsymbol{N}$ is the explicit part. They are converted back and forth between real space and Fourier space representations [5].

For this study, the implicit part is diagonal: $L_i = k^2 A_i y_i$, with $A = \left(\sigma + \kappa k^2, \kappa c_1^2 + 2\chi_{13}\lambda^2 k^2, 2\chi_{23}\lambda^2 k^2\right)$. All the other terms in the equation are encompassed in the explicit part $\boldsymbol{N}$. Thus, the update rule reads:

$$y_i^{n+1}(\boldsymbol{k}) = \frac{y_i^n(\boldsymbol{k}) + N_i[y_i^n(\boldsymbol{k})]}{1 + A_i k^2 \Delta t}. \tag{S39}$$

To improve the accuracy, we also perform m_{pc} predictor-corrector iterations for each time step:

$$y_i^{n+1,j+1}(\boldsymbol{k}) = \frac{y_i^n(\boldsymbol{k}) + \frac{1}{2}\left(N_i[y_i^n(\boldsymbol{k})] + N_i\left[y_i^{n+1,j}(\boldsymbol{k})\right]\right)}{1 + A_i k^2 \Delta t}, \tag{S40}$$

where j labels the predictor-corrector iterations with $y_i^{n+1,0} = y_i^n$ and $y_i^{n+1} = y_i^{n+1,m_{pc}}$.

The typical parameters used in this work are $L = 1000\lambda$, $N = 512$, $\Delta t = 1$, $m_{pc} = 3$.

III. TEMPERATURE DEPENDENCE OF THE PATTERNS

Here, we assume that the material properties and the interaction energies do not vary strongly with temperature. Thus, the temperature dependence predominantly enters through the entropy term. Since energy is measured in units of nk_BT, the rescaled parameters $(\bar{\sigma}, \bar{\kappa}, \chi, \xi)$ scale with temperature with a factor of $1/(k_BT)$. In the simulations, we tune temperature by rescaling these parameters by a factor of $\frac{T_0}{T}$, where T_0 is the reference temperature. Fig. S3 shows that the coarsening is arrested at a finite length scale (left), which decreases with temperature (right). Fig. S4 shows the hysteresis of the pattern morphology with respect to temperature. As the temperature is decreased, the

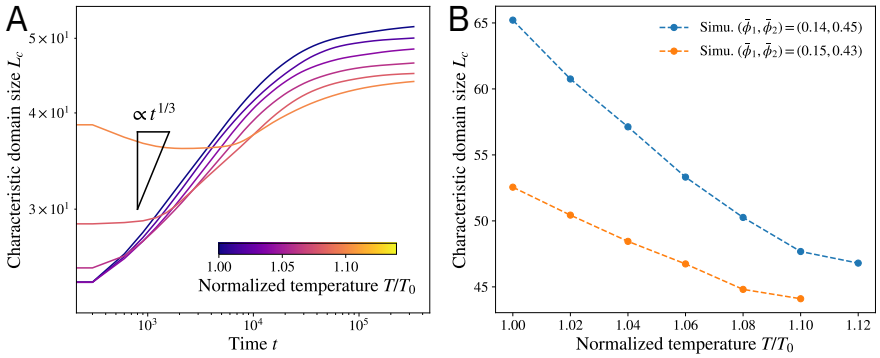

FIG. S3. (A) The time evolution of the characteristic domain size for different temperatures T. Mean composition: $(\bar{\phi}_1, \bar{\phi}_2) = (0.38, 0.36)$. All the other parameters are the same as in Fig. 1 of the main text. (B) The characteristic domain size at long times as a function of the temperature T. Both time and length are non-dimensionalized as described in the main text. T_0 is the reference temperature used in the non-dimensionalization.

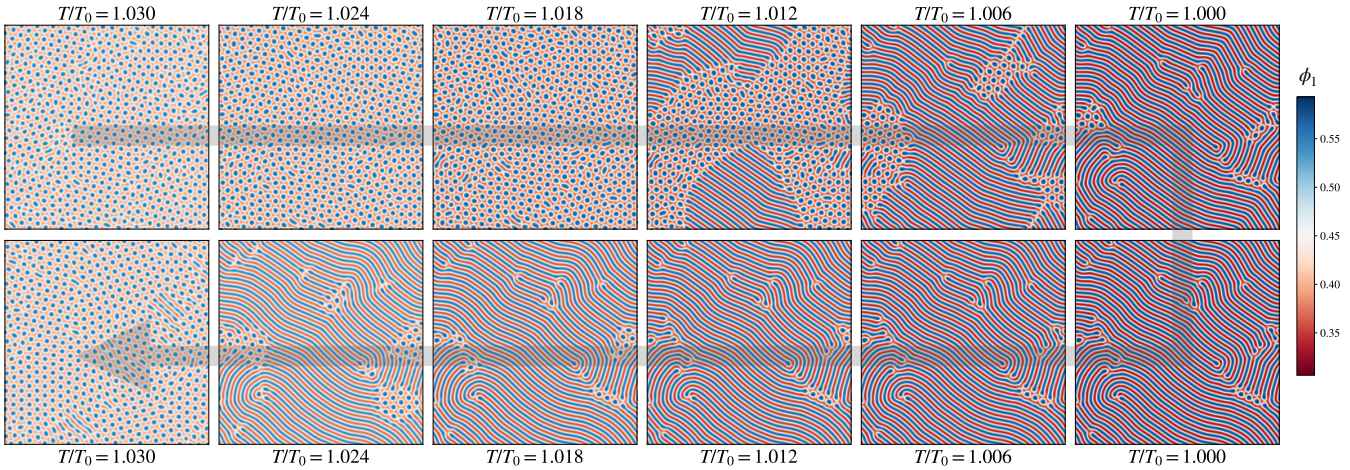

FIG. S4. Pattern hysteresis with respect to temperature. The temperature is first decreased and then increased according to the black arrow. Mean composition: $(\bar{\phi}_1, \bar{\phi}_2) = (0.45, 0.40)$. All the other parameters are the same as in Fig. 1 of the main text.

pattern starts to morph from the dot state to the stripe state at $T/T_0 \approx 1.012$, while the backward transition does not occur until $T/T_0 \approx 1.024$.

REFERENCES

[1] S. Mao, D. Kuldinow, M. P. Haataja, and A. Košmrlj, Phase behavior and morphology of multicomponent liquid mixtures, Soft Matter **15**, 1297 (2019).

[2] U. Thiele, A. J. Archer, M. J. Robbins, H. Gomez, and E. Knobloch, Localized states in the conserved Swift-Hohenberg equation with cubic nonlinearity, PHYSICAL REVIEW E **87**, 042915 (2013).

[3] P. C. Matthews and S. M. Cox, Pattern formation with a conservation law, Nonlinearity **13**, 1293 (2000).

[4] S. M. Cox, The envelope of a one-dimensional pattern in the presence of a conserved quantity, Physics Letters A **333**, 91 (2004).

[5] J. W. Cooley, P. A. W. Lewis, and P. D. Welch, The Fast Fourier Transform and Its Applications, IEEE TRANSACTIONS ON EDUCATION (1969).